Derivation of Equivalent Circuit Rotor Current from Rotor Bar Current Measurements in Brushless Doubly-Fed Machine

Ehsan Abdi, *Senior Member, IEEE,* Salman Abdi, *Senior Member, IEEE,* Richard McMahon, and Peter Tavner, *Senior Member, IEEE*

Abstract— This paper presents a method to estimate the BDFM equivalent circuit rotor current from rotor bar current measurements. Rotor currents are measured using a specially designed hardware that incorporates Rogowski coils and Bluetooth wireless transmission. The measurement of rotor currents enables the parameters in the BDFM's full equivalent circuit to be extracted unambiguously. In particular, stator and rotor leakage inductances can be estimated from experimental tests, which was not possible before from terminal measurement. The method is presented for a nested-loop rotor design and experimental measurements are shown for a prototype D180 frame BDFM

Index Terms— Brushless doubly-fed machine, Nested-loop rotor, Equivalent circuit model, Rotor current measurements, Rogowski coils, Curve fitting methods, Wind energy.

I. INTRODUCTION

The Brushless Doubly-Fed induction Machine (BDFM) is an attractive proposition for variable speed applications, especially in wind power generation [1], [2]. Several experimental BDFMs have been built ranging from small laboratory sizes up to several hundreds of kilowatts including a 250 kW size built by the authors [3], [4] and most recently, an 800 kW machine built for hydropower generation by Chen et al. [5]. Research on the BDFM has gained a fresh momentum in recent years which has led to significant improvement in the understanding, design and control of the machine [6]–[23].

The BDFM is a single-frame induction machine with two three-phase stator windings of different pole numbers that do not couple to each other directly. The coupling takes place through a specially-designed rotor that couples to both stator fields. The BDFM rotor is thus an important component of the machine as its winding carries the magnetic motive force (MMF) induced by both stator windings. Typically, one stator winding, called the power winding (PW), is connected to the mains and the other, called the control winding (CW) is supplied through a partially rated converter [24], [25]. The BDFM's desirable operation is in the synchronous mode where the shaft speed is determined by the stator supply frequencies [26], [27].

The vast majority of experimental BDFMs have utilised a nested-loop design for the rotor, which comprises symmetrical nests each containing one or several concentric loops [3], [14]–[16], [28]–[37]. The loops are often made of solid bars which are shorted at one end of the rotor with a common end ring. Alternative rotor designs, such as the bar cage rotor with internal loops [32], [38], [39], hybrid rotor [40] and wound rotor [41], [42] have also been studied for the BDFM.

The BDFM can be thought of two induction machines of different pole numbers with their rotors connected both mechanically and electrically [43]. The equivalent circuit model of the BDFM, shown in Fig. 1(a), essentially represents this cascade configuration [44], [45]. The equivalent circuit is a simple tool to work out the steady state performance measures of the BDFM and can be utilised in iterative machine design optimisation [46], converter rating optimisation [47], [48], and to understand the machine's operating limits [49]. The parameter values may be affected by the rotational speed and exerted load, however, these effects are generally negligible and can be neglected for the majority of machine analyses [50].

Several studies have attempted to integrate iron losses into the equivalent circuit model of the BDFM [31], [51]. However, as highlighted in these works, calculating iron losses in the BDFM is challenging due to its complex and nonlinear magnetic fields. Consequently, equivalent circuit models have struggled to accurately predict these losses. Recent research indicates that numerical methods, particularly finite element analysis, offer a more accurate approach for estimating BDFM core losses [7], [52]. In the present study, the impact of iron losses in the equivalent circuit model is not taken into account.

In experimental BDFMs, obtaining precise estimations of the equivalent circuit parameters is valuable to ensure the validation of theoretical designs and achieve accurate predictions of machine performance. This is of particular benefit to machine manufacturers and researchers studying prototype BDFMs. The equivalent circuit parameters may be calculated from the machine's geometrical dimensions and materials specifications using analytical methods, such as the coupled circuit and winding factor methods [50]. However, the accuracy of these calculations depends on having precise geometrical data for the machine. There are particular limitations with the accurate measurement of the air gap, which directly affects

E. Abdi is with Wind Technologies Limited, Cambridge CB4 0WS, UK (e-mail: ehsan.abdi@windtechnologies.com).

S. Abdi is with with the School of Engineering, University of East Anglia (UEA), Norwich NR4 7TJ, UK (e-mail: s.abdi-jalebi@uea.ac.uk).

Richard McMahon is with the Warwick Manufacturing Group (WMG), University of Warwick, Coventry CV4 7AL, UK (e-mail: r.mcmahon.1@warwick.ac.uk).

Peter Tavner is with the School of Engineering and Computing Sciences, Durham University, Durham DH1 3LE, UK (e-mail:peter.tavner@durham.ac.uk).

the inductances in the equivalent circuit. In addition, it is hard to obtain precise estimates of certain parameters such as the leakage reactances of end-windings.

An alternative approach for estimating the BDFM equivalent circuit parameters involves utilising curve-fitting methods applied to experimental tests [44] or Finite Element (FE) results [53], [54]. These methods have demonstrated superior accuracy in parameter estimation, but with a limitation: they were only able to extract parameters for a simplified, yet electrically equivalent, form of the equivalent circuit shown in Fig. 1(b) [44]. This limitation arises due to challenges in measuring rotor bar currents and their subsequent conversion to the equivalent circuit rotor current, which result in electrical measurements being confined to 'terminal' quantities (i.e. stator windings). As a result, it was not possible to unambiguously determine all the inductance values in the 'full' equivalent circuit shown in Fig. 1(a) [44]. Thus, instead of obtaining three distinct inductances L_r, L_1 and L_2 in the 'full' model, a single inductance parameter $\hat{L}_r$ is derived in the simplified model, representing the combined effects of L_r, L_1 and L_2.

Having specific knowledge of the rotor inductance (L_r) is highly advantageous, as it allows for the evaluation of different rotor designs and optimisation of various performance aspects, including reactive power management [55], converter rating [10] and machine behaviour during grid low-voltage ride-through (LVRT) events [56]. To obtain L_r accurately through curve-fitting methods applied to experimental tests, it is necessary to measure rotor bar currents and subsequently convert them to the equivalent circuit rotor current. In previous studies [57], [58], an instrumentation apparatus incorporating Rogowski coils for current measurements and Bluetooth for wireless data transmission was implemented. However, the conversion of rotor bar currents to the equivalent circuit rotor current remains an unexplored area of research.

This paper presents two important contributions to the study of the BDFM. Firstly, it presents an analytical method to estimate the equivalent circuit rotor current from rotor bar current measurements in a nested-loop rotor. Secondly, leveraging the method outlined and the hardware detailed in [58], it derives distinct values for L_r, L_1 and L_2 in the 'full' equivalent circuit shown in Fig. 1(a). These parameters are subsequently utilised to predict the performance of the BDFM, and the predictions are validated through experimental verification.

II. Transforming Rotor Loop Currents into Equivalent Circuit Rotor Current

Fig. 2 shows the sequence of transformations required to obtain the equivalent circuit rotor current from measured rotor loop currents in steady state conditions. The transformations are described here for a general class of nested-loop rotors with $S = p_1 + p_2$ nests, each comprising N concentric loops. p_1 and p_2 are the pole pairs of stator 1 and stator 2, respectively. To clarify the terminology, consider Fig. 3 which is a nested-loop design for a 2/4 pole pair BDFM. The rotor has six nests ($S = 6$). Each nest comprises three concentric loops ($N = 3$):
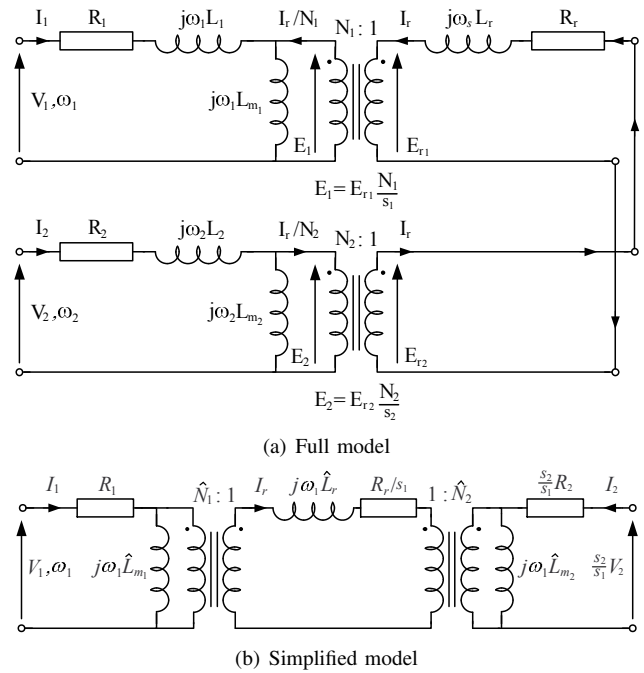

(a) Full model

(b) Simplified model

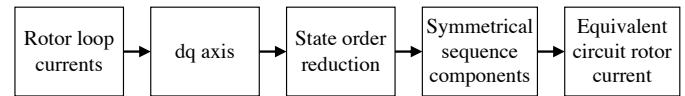Fig. 1.   BDFM per-phase equivalent circuit

Fig. 2.   Transformations required to obtain the equivalent circuit rotor current from measured rotor loop currents

inner, middle and outer loops. Therefore, there are three sets of similar loops i.e. six inner loops, six middle loops and six outer loops.

A. dq Transformation

Since the rotor cannot simply be presented as a three-phase system, an appropriate *dq* transformation must be used for the rotor currents. For a nested-loop rotor with S nests, a *dq* transformation matrix was proposed in [59] which is similar to that of an S-phase system. It was also shown in [59] that the transformation can be represented for either p_1 or p_2 pole pairs. The following transformation for p_1 pole pairs is used for one set of S similar loops (e.g. the set of six middle loops in Fig. 3):

$$\mathbf{C}_{dq} = \sqrt{\frac{2}{S}} \begin{bmatrix} \cos(0) & \cos(\frac{2\pi p_1}{S}) & ... & \cos(\frac{2\pi(S-1)p_1}{S}) \\ \sin(0) & \sin(\frac{2\pi p_1}{S}) & ... & \sin(\frac{2\pi(S-1)p_1}{S}) \end{bmatrix} \quad (1)$$

The transformation of loop currents into *dq* currents is thus given by:

$$\mathbf{i}_{dq} = \mathbf{C}_{dq}\mathbf{i}_r \quad (2)$$

where $\mathbf{i}_r \in \mathbb{R}^S$ comprises the loop currents and $\mathbf{i}_{dq_r} \in \mathbb{R}^2$ is the *dq* currents.

In any balanced S-phase system, at steady-state operation, the quantities such as the currents have the same amplitude, with a suitable phase difference. This is physically justified due
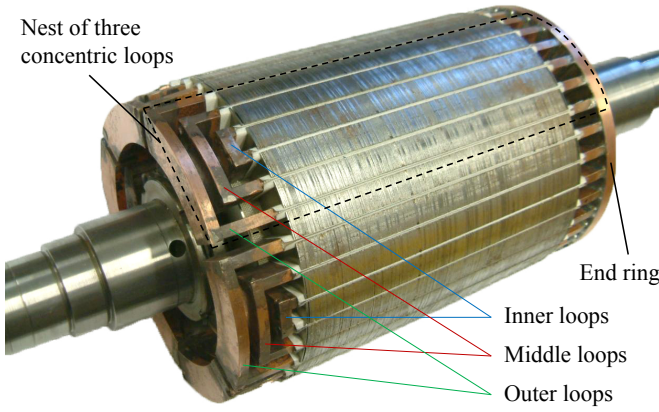
Fig. 3. A nested-loop design for a 2/4 pole pair BDFM

to the symmetrical geometry of the nested-loop rotor. Thus, at steady-state, measurements of only one current in each set of rotor loops is sufficient to derive the *dq* currents for that set. However, in order to preserve the system rank which is 2 for the *dq* model, the currents in at least two loops of each set (e.g. two inner loops, two middle loops, and two outer loops in the rotor shown in Fig. 3) must be included in the transformation [60, sect. 3.2]. This can be achieved by adding a suitable phase offset to a loop current in one nest to obtain the current of an identical loop in another nest:

$$\tilde{\mathbf{i}}_r = \mathbf{P}\mathbf{i}_r = \left[\begin{array}{c} I_R\angle\phi(t) \\ I_R\angle(\phi(t)+\theta_o) \end{array} \right] \quad (3)$$

where $\tilde{\mathbf{i}}_r \in \mathbb{R}^2$ comprises the currents in two identical loops of consecutive nests (e.g. the two inner loops shown in Fig. 3) and $\mathbf{P} \in \mathbb{R}^{2\times S}$ is a matrix which has a single 1 in each row, with all other elements zero, and is rank 2 (that is the 1s must be in different columns). I_R is the amplitude of the loop current, $\phi(t)$ is some arbitrary function of time and θ_o is an offset angle given by [61, sect. 3.3]:

$$\theta_o = \frac{2\pi}{p_1 + p_2} \gcd(p_1, p_2) \quad (4)$$

where $\gcd(p_1, p_2)$ is the greatest common divisor of p_1 and p_2.

Now, a transformation $\mathbf{C}_r \in \mathbb{R}^{2\times 2}$ is sought such that:

$$\mathbf{i}_{dq} = \mathbf{C}_r\tilde{\mathbf{i}}_r \quad (5)$$

From (3) and (5):

$$\mathbf{i}_{dq} = \mathbf{C}_r\mathbf{P}\mathbf{i}_r \quad (6)$$

Noting $\mathbf{C}_{dq}{}^T\mathbf{C}_{dq} = \mathbf{I}_{2\times 2}$ [60, sect. 3.2], from (2):

$$\mathbf{i}_r = \mathbf{C}_{dq}{}^T\mathbf{i}_{dq} \quad (7)$$

From (6) and (7):

$$\mathbf{i}_{dq} = \mathbf{C}_r\mathbf{P}\mathbf{C}_{dq}{}^T\mathbf{i}_{dq} \quad (8)$$

As $\mathbf{C}_r\mathbf{P}\mathbf{C}_{dq}{}^T$ is full rank, then:

$$\mathbf{C}_r\mathbf{P}\mathbf{C}_{dq}{}^T = \mathbf{I}_{2\times 2}$$
$$\Rightarrow \mathbf{C}_r = \left(\mathbf{P}\mathbf{C}_{dq}{}^T\right)^{-1} \quad (9)$$

Therefore, for a single set of S rotor loops (e.g. the six middle loops in Fig. 3), $\mathbf{C}_r \in \mathbb{R}^{2\times 2}$ determines the rotor *dq* currents from knowing two loop currents (with a suitable choice of $\mathbf{P}$).

For a nested-loop rotor with N loops per nest (i.e. N sets of S identical loops), the *dq* transformation matrix for rotor currents, $\mathbf{C}_{dq_r} \in \mathbb{R}^{2N\times 2N}$, is given by:

$$\mathbf{C}_{dq_r} = \left[\begin{array}{ccc} \mathbf{C}_r & \mathbf{0} & \mathbf{0} \\ \mathbf{0} & \ddots & \mathbf{0} \\ \mathbf{0} & \mathbf{0} & \mathbf{C}_r \end{array} \right] \quad (10)$$

where $\mathbf{C}_r$ is of the form of (9).

B. Rotor State Order Reduction

An important step to derive a single equivalent circuit rotor current from the measurement of currents in a multi-loop per nest rotor is to reduce the order of rotor states from N *dq* pairs to a single *dq* pair. In other words, we wish to find a simplified model of the rotor which is equivalent in complexity to the special case when the rotor comprises of only a single loop per nest. Physically speaking, we are trying to find a single set of rotor loops which reasonably approximate the performance of the true rotor which has multiple loops per nest.

Roberts et al. [59] proposed a model order reduction method for the nested-loop rotor and showed experimentally that the method has acceptable accuracy. McMahon et al. [50] subsequently used the same approach to calculate the BDFM equivalent circuit parameters from the coupled circuit equations, and reported close agreement with experimental and finite element results. Using the method described in [59], the order of rotor *dq* currents may be reduced to a single pair by:

$$\tilde{\mathbf{i}}_{dq_r} = \mathbf{T}_1^T\mathbf{i}_{dq_r} \quad (11)$$

where $\mathbf{i}_{dq_r} \in \mathbb{R}^{2N}$ comprises N *dq* pairs of rotor currents (e.g. three *dq* pairs for the rotor shown in Fig. 3, corresponding to inner, middle and outer loops), and $\tilde{\mathbf{i}}_{dq_r} \in \mathbb{R}^2$ is the approximated single pair of rotor *dq* currents. $\mathbf{T}_1 \in \mathbb{R}^{2N\times 2}$ is the eigenvector that corresponds to the largest eigenvalue of the rotor inductance matrix in the *dq* model. For details about how $\mathbf{T}_1$ is calculated, refer to [59].

C. Symmetrical Sequence Components

The single pair of rotor *dq* current may be transformed into positive and negative sequence components using the following transformation [62, sect. 3.7]:

$$\left[\begin{array}{c} i_r{}^+ \\ i_r{}^- \end{array} \right] = \mathbf{C}_s\tilde{\mathbf{i}}_{dq_r} = \mathbf{C}_s \left[\begin{array}{c} \tilde{i}_{d_r} \\ \tilde{i}_{q_r} \end{array} \right] \quad (12)$$

where:

$$\mathbf{C}_s = \frac{1}{\sqrt{2}} \left[\begin{array}{cc} 1 & j \\ 1 & -j \end{array} \right] \quad (13)$$

Under balanced three-phase conditions, the positive and negative sequence components are related as [60, sect. 4.2]:

$$i_r{}^+ = \bar{i_r{}^-} \quad (14)$$

Therefore, either of positive or negative sequence components may be utilised to derive the equivalent circuit rotor current.

Considering the positive sequence component, the transformation for the rotor current is:

$$i_r{}^+ = \mathbf{C}_s^+ \tilde{\mathbf{i}}_{dq_r} \tag{15}$$

where:

$$\mathbf{C}_s^+ = \frac{1}{\sqrt{2}} \begin{bmatrix} 1 & j \end{bmatrix} \tag{16}$$

It was shown in [60, sect. 4.2] that under steady state conditions, $i_r{}^+$ will become I_r in the equivalent circuit shown in Fig. 1(a).

D. Equivalent Circuit Rotor Current

Noting that the *dq* and symmetrical sequence components transformations will magnify the phase voltage and current quantities by a factor of $\sqrt{\frac{3}{2}}$, and assuming $\phi(t) = 0$ in (3), the rotor current in the equivalent circuit can be obtained from the measurement of rotor loop currents using (10), (11) and (16):

$$I_r = \sqrt{\frac{2}{3}} \mathbf{C}_s^+ \mathbf{T}_1^T \mathbf{C}_{dq_r} \begin{bmatrix} \begin{bmatrix} 1 \\ cos(\theta_o) \end{bmatrix} I_{R_1} \\ \begin{bmatrix} 1 \\ cos(\theta_o) \end{bmatrix} I_{R_2} \\ \vdots \\ \begin{bmatrix} 1 \\ cos(\theta_o) \end{bmatrix} I_{R_N} \end{bmatrix} \tag{17}$$

where $I_{R_1}, I_{R_2}, \ldots, I_{R_N}$ are the amplitude of the measured rotor loop currents in a single nest (e.g. inner, middle and outer loop currents in a single nest in Fig. 3).

III. EXPERIMENTAL SETUP

The specifications of the prototype BDFM is given in Table I and the test rig is shown in Fig. 4. The BDFM is mechanically coupled to a DC drive (ABB DCS800) which enables running the BDFM as a motor or generator. The mechanical coupling is through HBM T30FN torque transducer. The shaft speed is measured using an incremental encoder with a resolution of 2500 cycles/rev. The stator voltages and currents are measured by LEM LV 25-p and LEM LTA 100-p transducers with measurement accuracies 0.9% and 0.5%, respectively.

Rotor loop currents are sensed using Rogowski coils [63], [64]. After an analogue integration, the output is digitised and transmitted from the rotor to a PC using a wireless link, as shown in Fig. 5(a) [58], [65], [66]. The measurement setup comprises the elements shown in Fig. 5(b) and its installation is shown in Fig. 5(c). It can measure bar currents up to 3000 A with resolution of $<1\%$, from 1 to 100 Hz. The system is powered by rechargeable batteries. Recharging *in situ* is possible via connections brought out through a hole in the shaft. Reading from four Rogowski coils are used to measure the end ring currents at four locations, as shown in Fig. 5(b). The rotor loop currents shown in Fig. 6 can be obtained from the measured end ring currents as:

$$\begin{aligned} i_{l_1} &= i_{r_1} - i_{r_2} \\ i_{l_2} &= i_{r_2} - i_{r_3} \\ i_{l_3} &= i_{r_3} - i_{r_4} \end{aligned} \tag{18}$$

TABLE I
SPECIFICATIONS OF THE EXPERIMENTAL BDFM

| Parameters	Value
Frame size	D180
PW/CW pole pairs	2/4
Natural speed	500 rpm
PW rated voltage	240 V (50 Hz, delta)
PW rated current	13 A (line)
CW rated voltage	240 V (30 Hz, delta)
CW rated current	13 A (line)
Rated torque	100 Nm
Stator slot number	48
Rotor slot number	36
Rotor design	Nested-loop design consisting of 6 nests of 3 concentric loops of pitch 5/36, 3/36 and 1/36 of the rotor circumference. Each nest offset by 1/6 of the circumference.
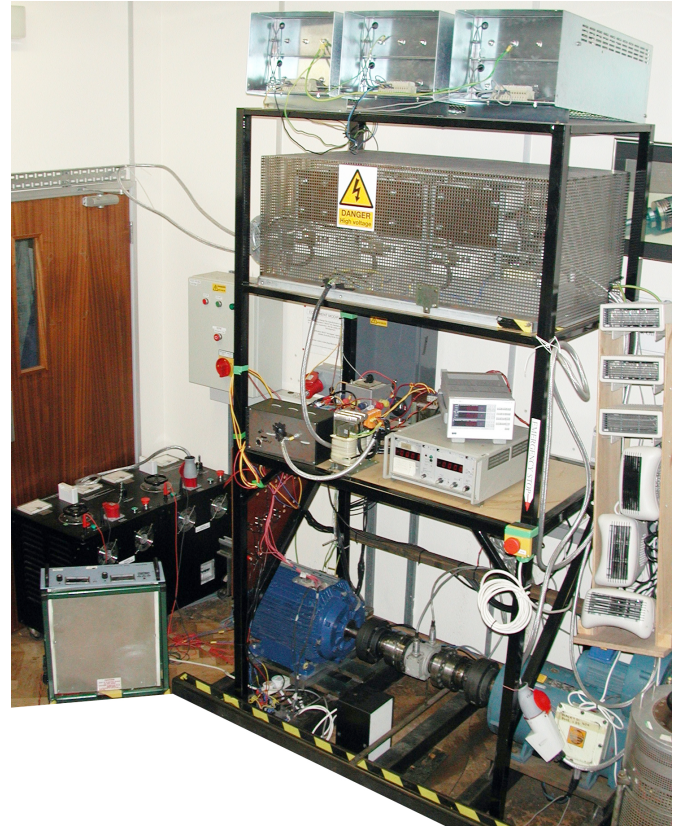
Fig. 4. Prototype D180 frame BDFM (left) on the test rig

IV. EQUIVALENT CIRCUIT PARAMETER ESTIMATION

The procedure adopted to estimate the equivalent circuit parameters from experimental measurements is shown in Fig. 7. This procedure builds upon the previously proposed approach in [50] by incorporating rotor current measurements into the experimental data, thus extending its ability to estimate L_r, L_1 and L_2 in the full equivalent circuit shown in Fig. 1(a).

The stator winding resistances were obtained from DC measurements at 80 °C. The sums of stator winding leakage and magnetising inductances, $L_1 + L_{m_1}$ and $L_2 + L_{m_2}$, were
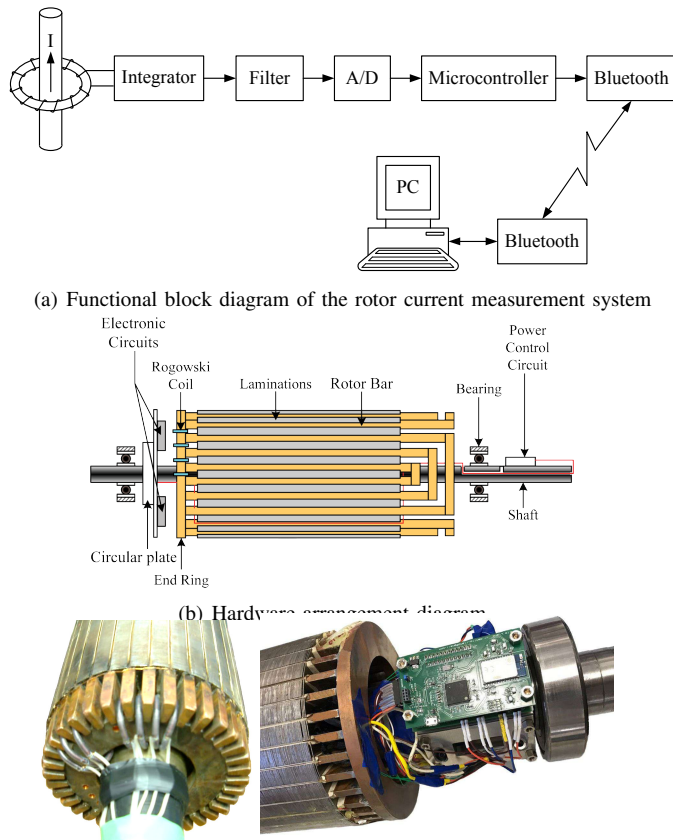
This article has been accepted for publication in IEEE Transactions on Energy Conversion. This is the author's version which has not been fully edited and content may change prior to final publication. Citation information: DOI 10.1109/TEC.2024.3395903

5

(a) Functional block diagram of the rotor current measurement system

(b) Hardware arrangement diagram

(c) Installation of Rogowski coils and electronic hardware

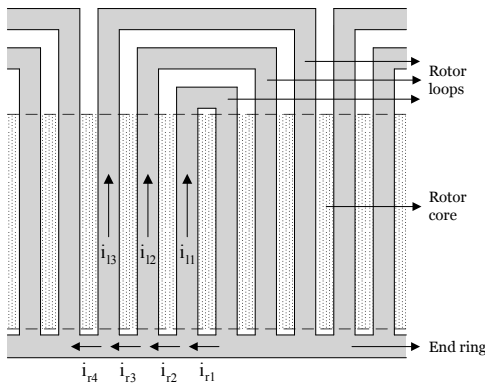Fig. 5. Rotor current measurement system [63]

Fig. 6. End ring and loop currents in a nested-loop design

derived from no-load tests conducted at 90 V, 50 Hz.

Two cascade tests were conducted: one with the 4-pole winding supplied at 90 V, 50 Hz and the 8-pole winding shorted, and one with the 8-pole winding supplied at 110 V, 50 Hz and the 4-pole winding shorted. The supply voltages were chosen to limit the stator currents to acceptable values and to avoid saturation in the iron circuit. The BDFM was run over the speed range of 0-1500 rpm and approximately twenty operating points were logged in each cascade test. For each operating point, the stator voltages, currents and power factors, rotor loop currents, mechanical speed and torque were measured at steady state.

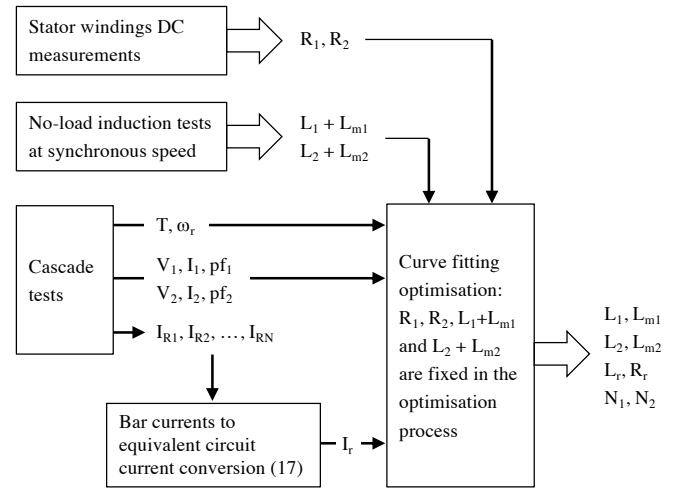The rotor loop currents were converted to the equivalent

Fig. 7. Equivalent circuit parameter estimation procedure from experimental tests
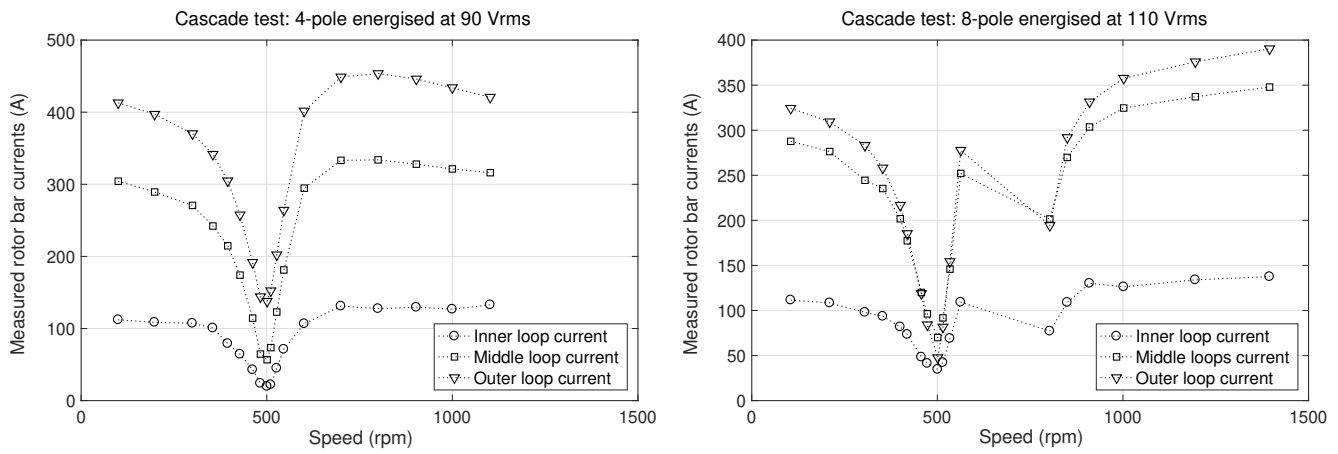
circuit rotor current (I_r) using the method outlined in section II. Then, the transformed rotor current, together with stator measurements, mechanical speed, and torque, were fed into the curve-fitting optimisation process to estimate the parameters of the equivalent circuit [44], [53]. Fig. 8 shows the measured torque and rotor loop currents in the cascade tests, along with the transformed equivalent circuit rotor current. The best-fitted curve to the torque and transformed rotor current data points are also depicted in Fig. 8.

Table II displays the parameter values for the 'full' equivalent circuit depicted in Fig. 1(a). The table includes two sets of parameters: one estimated using the curve-fitting method described earlier, and the other calculated based on the machine's geometric dimensions using the method proposed in [50]. The disparity between the two parameter sets is less than 10%. Notably, the most significant discrepancies are observed in the stator and rotor leakage inductance values, which is to be expected due to the intricacies involved in calculating leakage inductance, particularly in the BDFM with complex magnetic field distributions [53].

TABLE II

EQUIVALENT CIRCUIT PARAMETERS FOR THE PROTOTYPE D180 BDFM, DERIVED FROM THE EXPERIMENTAL METHOD DESCRIBED IN THIS PAPER AND THE ANALYTICAL METHOD PROPOSED IN [50]

Parameters	Experimental estimation	Analytical calculation	Difference
$R_1 (\Omega)$	2.4	2.3	4.2%
$L_1 (mH)$	4.9	4.4	10.2%
$L_{m_1} (mH)$	268	272	1.5%
$R_2 (\Omega)$	4.0	3.9	2.5%
$L_2 (mH)$	12.4	11.4	8.1%
$L_{m_2} (mH)$	274	276	0.7%
$R_r (\mu\Omega)$	96.9	95.4	1.5%
$L_r (\mu H)$	2.0	1.90	5.0%
N_1	115.4	112.4	2.6%
N_2	159.2	156.5	1.7%
N_1/N_2	0.725	0.718	1.0%

(a) Measured rotor loop currents, obtained from the hardware described in Section III
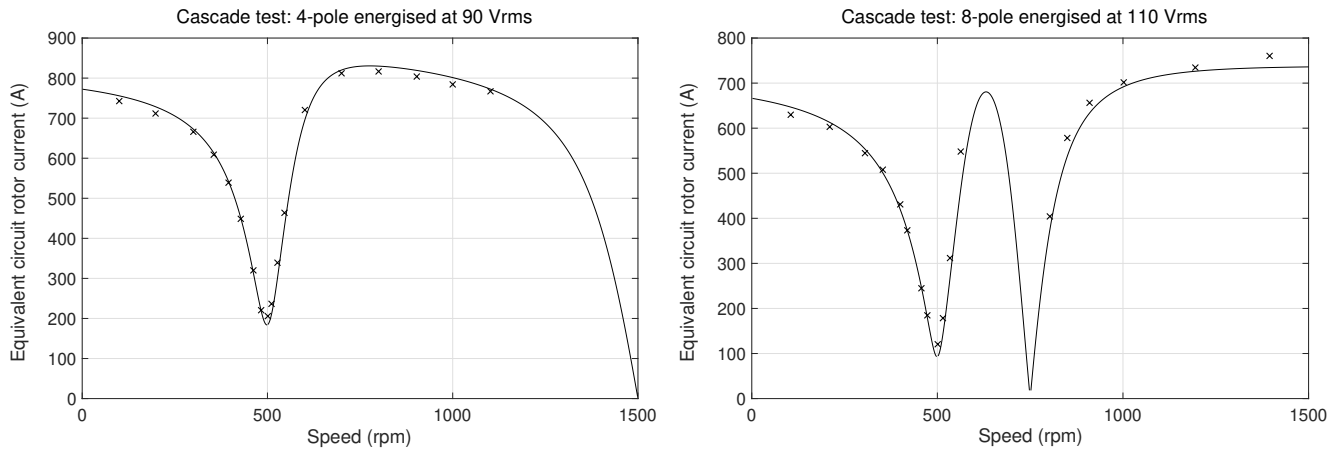
(b) Equivalent circuit rotor current derived from the transformation of measured rotor loop currents using the method described in II, overlaid with best-fitted curve
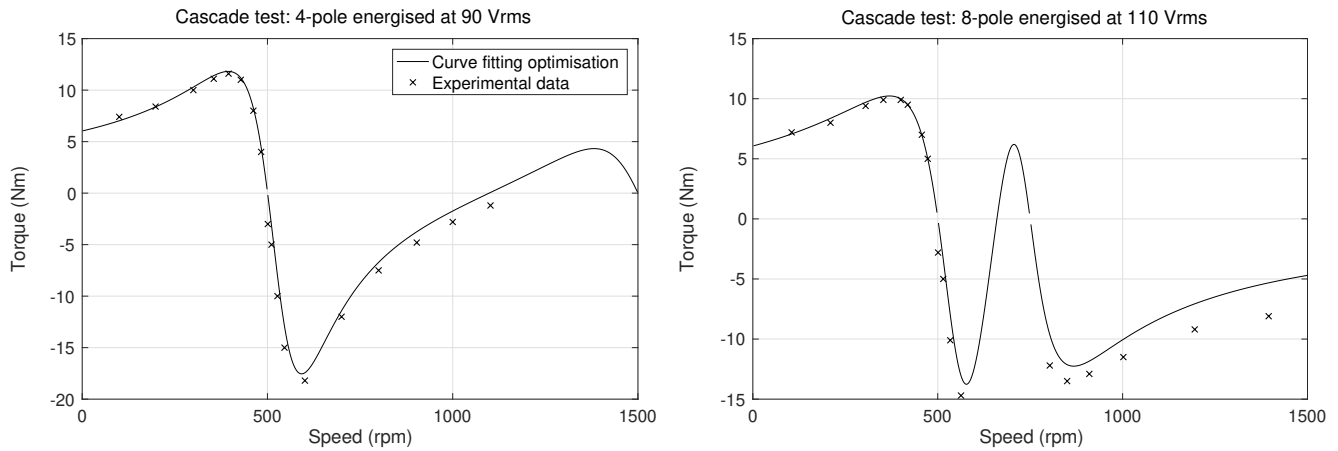
(c) Measured torque overlaid with best-fitted curve

Fig. 8. Measured torque (c) and rotor loop currents (a) obtained during the cascade tests, accompanied by the transformed equivalent circuit rotor current (b). The figure also depicts the best-fitted curves for the transformed rotor current and torque data points (b and c). These plots (b and c) are integral to the curve-fitting optimisation process used to estimate the equivalent circuit parameters listed in Table II.

V. STEADY STATE MODEL VERIFICATION

The equivalent circuit with parameters listed in Table II was utilised to predict the steady-state performance of the BDFM, providing an evaluation of the practicality and accuracy of the proposed parameter estimation method. To validate the predictions of the equivalent circuit, experimental tests were conducted in the synchronous mode of BDFM operation. The 4-pole stator winding (PW) was supplied with a constant voltage and frequency of 90 V, 50 Hz. The 8-pole stator winding (CW) was connected to a variable voltage, variable

frequency converter. The converter frequency was set at 30 Hz, corresponding to a shaft speed of 800 rpm. The converter voltage was varied from 70 V (under-excitation) to 160 V (over-excitation) which essentially allowed adjusting the reactive power in the PW [67].

The stator voltages were chosen at sub-rating levels to avoid saturation in the iron circuit. This was important in the verification process since the equivalent circuit, being a linear model, does not account for the effects of iron saturation [21]. With the chosen sub-rating stator voltages, the load torque applied by the DC drive was adjusted to 30 Nm to ensure that the stator currents remained within their specified ratings.

Fig. 9 presents the experimental results, overlaid with the equivalent circuit predictions generated using the two sets of parameters listed in Table II. Overall, all predictions fall within an acceptable range. However, it is worth noting that the parameters estimated from the experimental tests (the first set of parameters listed in Table II) exhibit closer agreement with the experimental results, as anticipated. These findings highlight the significance of both methods for determining the equivalent circuit parameters in the study of the BDFM. The analytical method proves valuable for iterative design optimisations, while the experimental method is crucial for characterising experimental machines and assessing their performance.

The measured rotor loop currents are shown in Fig. 10(a). The outer loop carries the highest and the inner loop the lowest currents, which signifies that the outer loop has the strongest overall coupling to the stator windings. Fig. 10(b) shows the equivalent circuit rotor current derived from transforming the measured loop currents as described in Section II. The overlaid predictions from the equivalent circuit models demonstrate a close agreement with the experimental measurements. These results highlight the practicality and acceptable accuracy of the transformation procedure proposed in Section II, particularly the state order reduction method.

VI. Conclusions

The equivalent circuit model serves as a valuable analytical tool for assessing the steady-state performance and operating limits of the BDFM. With each parameter holding a distinct physical meaning, the model proves particularly useful in design optimisation and the evaluation of different machine configurations.

The nested-loop rotor, characterised by multiple concentric loops per nest, poses a challenge in simplifying the BDFM equivalent circuit representation. This paper addresses this challenge by proposing a method to transform the rotor loop currents in the nested-loop design into the rotor current in the equivalent circuit model. This transformation enables the utilisation of rotor current measurements in the parameter estimation process, ensuring unambiguous derivation of all inductances in the 'full' equivalent circuit. While the approach is presented specifically for the nested-loop rotor, it can be extended to other rotor designs, such as the bar cage rotor with internal loops [32], [38].
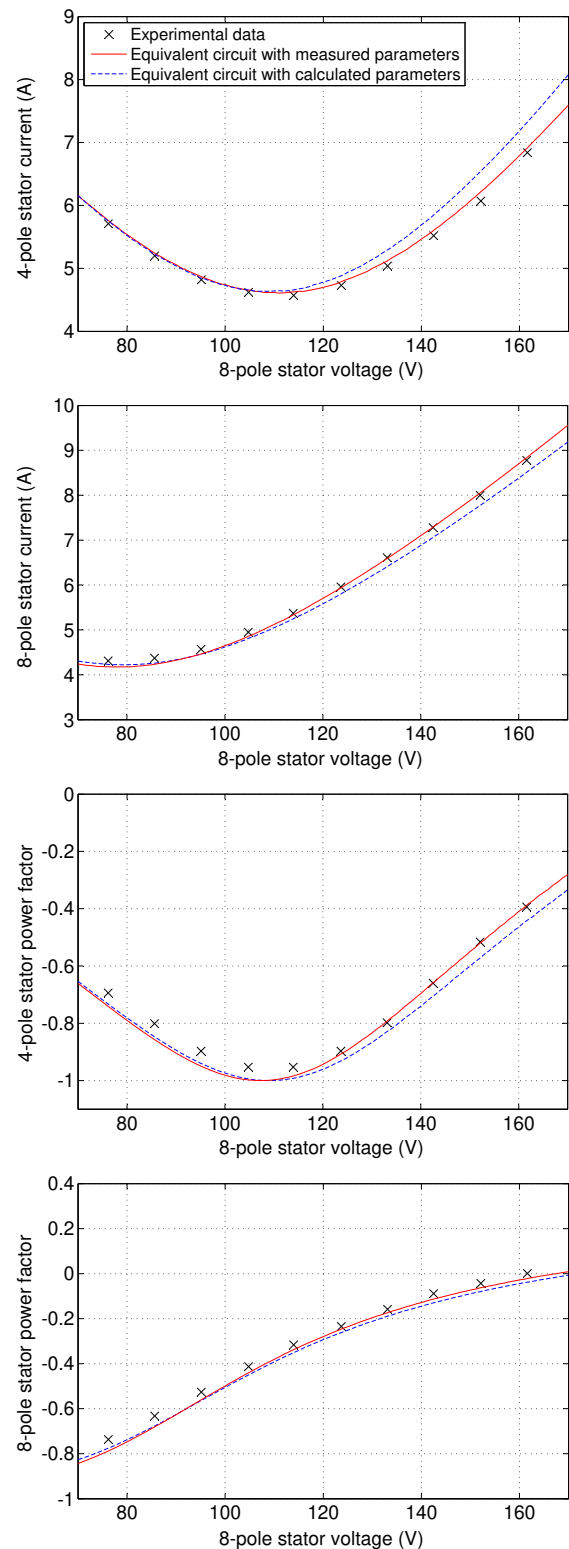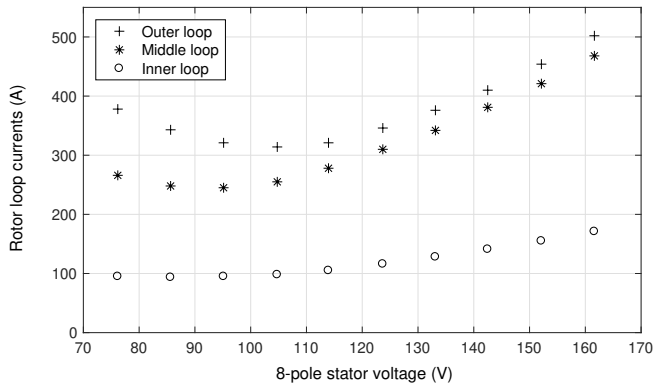

Fig. 9.   Experimental validation of equivalent circuit predictions for the BDFM operating in synchronous mode. The CW voltage was varied to adjust the PW reactive power. The measured experimental data are overlaid with predictions obtained from the equivalent circuit using both sets of parameters listed in Table II

References

[1] T. D. Strous, H. Polinder, and J. A. Ferreira, "Brushless doubly-fed induction machines for wind turbines: developments and research

This article has been accepted for publication in IEEE Transactions on Energy Conversion. This is the author's version which has not been fully edited and content may change prior to final publication. Citation information: DOI 10.1109/TEC.2024.3395903

8

(a) RMS values of measured rotor loop currents with Rogowski coils
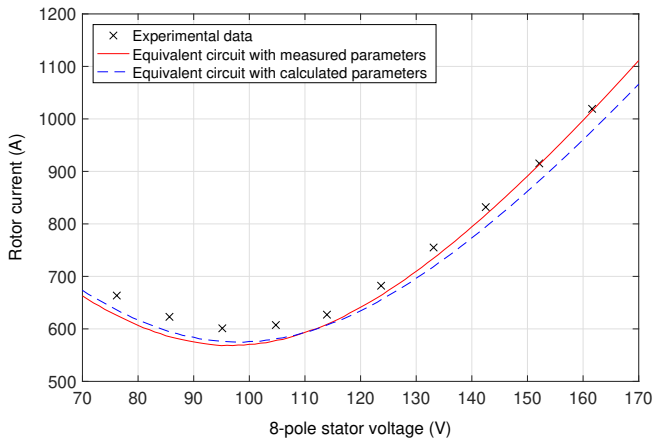
(b) Rotor current in the equivalent circuit: crosses (×) are derived from transforming the measured rotor loop currents (above) to the equivalent circuit rotor current. Overlaid lines are predictions from the equivalent circuit models.

Fig. 10. Experimental validation of the transformation procedure for converting rotor loop currents to the equivalent circuit rotor current

challenges," *IET Electric Power Applications*, vol. 11, no. 6, pp. 991–1000, 2017.

[2] E. Abdi, M. Tatlow, R. McMahon, and P. Tavner, "Design and performance analysis of a 6 mw medium-speed brushless dfig," in *2nd IET Renewable Power Generation Conference (RPG 2013)*, 2013, pp. 1–4.

[3] E. Abdi, R. McMahon, P. Malliband, S. Shao, M. E. Mathekga, P. Tavner, S. Abdi, A. Oraee, T. Long, and M. Tatlow, "Performance analysis and testing of a 250 kw medium-speed brushless doubly-fed induction generator," *IET Renewable Power Generation*, vol. 7, no. 6, pp. 631–638, 2013.

[4] S. Abdi, E. Abdi, and R. McMahon, "Experimental and finite element studies of a 250 kw brushless doubly fed induction generator," *The Journal of Engineering*, vol. 2019, no. 12, pp. 8489–8495, 2019.

[5] J. Chen, X. Wang, T. Zhao, Z. Li, M. Kong, and P. Nie, "Application of brushless doubly-fed machine system in hydropower generation," in *22nd International Conference on Electrical Machines and Systems (ICEMS)*, 2019, pp. 1–4.

[6] H. Mosaddegh Hesar, M. A. Salahmanesh, and H. A. Zarchi, "Generalized analysis of brushless doubly fed induction machine taking magnetic saturation and iron loss into account," *IEEE Transactions on Industrial Electronics*, vol. 68, no. 8, pp. 6470–6480, 2021.

[7] S. Abdi, E. Abdi, and R. Mcmahon, "A new iron loss model for brushless doubly-fed machines with hysteresis and field rotational losses," *IEEE Transactions on Energy Conversion*, pp. 1–1, 2021.

[8] J. Su, Y. Chen, D. Zhang, and Y. Kang, "Full-parameter identification model based on back propagation algorithm for brushless doubly fed induction generator," *IEEE Transactions on Power Electronics*, vol. 35, no. 10, pp. 9953–9958, 2020.

[9] Y. Cheng, B. Yu, C. Kan, and X. Wang, "Design and performance study of a brushless doubly fed generator based on differential modulation,"

[10] A. Oraee, E. Abdi, and R. McMahon, "Converter rating optimisation for a brushless doubly fed induction generator," *IET Renewable Power Generation*, vol. 9, no. 4, pp. 360–367, 2015.

[11] O. M. E. Mohammed, W. Xu, Y. Liu, and F. Blaabjerg, "An improved control method for standalone brushless doubly fed induction generator under unbalanced and nonlinear loads using dual-resonant controller," *IEEE Transactions on Industrial Electronics*, vol. 68, no. 7, pp. 5594–5605, 2021.

[12] S. Shao, E. Abdi, and R. McMahon, "Stable operation of the brushless doubly-fed machine (bdfm)," in *7th International Conference on Power Electronics and Drive Systems*, 2007, pp. 897–902.

[13] J. Yang, W. Tang, G. Zhang, Y. Sun, S. Ademi, F. Blaabjerg, and Q. Zhu, "Sensorless control of brushless doubly fed induction machine using a control winding current mras observer," *IEEE Transactions on Industrial Electronics*, vol. 66, no. 1, pp. 728–738, 2019.

[14] U. Shipurkar, T. D. Strous, H. Polinder, J. A. Ferreira, and A. Veltman, "Achieving sensorless control for the brushless doubly fed induction machine," *IEEE Transactions on Energy Conversion*, vol. 32, no. 4, pp. 1611–1619, 2017.

[15] J. Chen, W. Zhang, B. Chen, and Y. Ma, "Improved vector control of brushless doubly fed induction generator under unbalanced grid conditions for offshore wind power generation," *IEEE Transactions on Energy Conversion*, vol. 31, no. 1, pp. 293–302, 2016.

[16] A. Zhang, Z. Chen, R. Gao, J. Wang, Z. Ma, S. Wang, and Y. Wang, "Crowbarless symmetrical low-voltage ride through based on flux linkage tracking for brushless doubly fed induction generators," *IEEE Transactions on Industrial Electronics*, vol. 67, no. 9, pp. 7606–7616, 2020.

[17] T. Long, S. Shao, E. Abdi, P. Malliband, M. E. Mathekga, R. A. McMahon, and P. J. Tavner, "Symmetrical low voltage ride-through of a 250 kw brushless dfig," in *6th IET International Conference on Power Electronics, Machines and Drives (PEMD 2012)*, 2012, pp. 1–6.

[18] S. Abdi, E. Abdi, and R. McMahon, "A study of unbalanced magnetic pull in brushless doubly fed machines," *IEEE Transactions on Energy Conversion*, vol. 30, no. 3, pp. 1218–1227, 2015.

[19] S. Abdi, E. Abdi, H. Toshani, and R. McMahon, "Vibration analysis of brushless doubly fed machines in the presence of rotor eccentricity," *IEEE Transactions on Energy Conversion*, vol. 35, no. 3, pp. 1372–1380, 2020.

[20] S. Abdi, E. Abdi, A. Oraee, and R. A. McMahon, "Investigation of magnetic wedge effects in large-scale bdfms," in *2nd IET Renewable Power Generation Conference (RPG 2013)*, 2013, pp. 1–4.

[21] E. Abdi, P. Malliband, and R. McMahon, "Study of iron saturation in brushless doubly-fed induction machines," in *IEEE Energy Conversion Congress and Exposition*, 2010, pp. 3501–3508.

[22] S. Shao, E. Abdi, and R. McMahon, "Operation of brushless doubly-fed machine for drive applications," in *4th IET Conference on Power Electronics, Machines and Drives*, 2008, pp. 340–344.

[23] S. Abdi, E. Abdi, R. A. McMahon, and E. Abtahizadeh, "Analytical study of rotor eccentricity effects on brushless doubly fed machines vibration," in *International Conference on Electrical Machines (ICEM)*, vol. 1, August 2020, pp. 1855–1861.

[24] R. McMahon, X. Wang, E. Abdi-Jalebi, P. Tavner, P. Roberts, and M. Jagiela, "The bdfm as a generator in wind turbines," in *12th International Power Electronics and Motion Control Conference*, 2006, pp. 1859–1865.

[25] E. Abdi, R. A. McMahon, and P. J. Tavner, "Brushless doubly fed machines," US Patent App. 14/131,958, 2014.

[26] S. Tohidi, "Analysis and simplified modelling of brushless doubly-fed induction machine in synchronous mode of operation," *IET Electric Power Applications*, vol. 10, no. 2, pp. 110–116, 2016.

[27] E. Abdi, X. Wang, S. Shao, R. A. McMahon, and P. J. Tavner, "Performance characterisation of brushless doubly-fed generator," in *IEEE Industry Applications Society Annual Meeting*, 2008, pp. 1–6.

[28] R. Li, R. Spee, A. K. Wallace, and G. C. Alexander, "Synchronous drive performance of brushless doubly-fed motors," *IEEE Transactions on Industry Applications*, vol. 30, no. 4, pp. 963–970, 1994.

[29] S. Williamson and A. C. Ferreira, "Generalised theory of the brushless doubly-fed machine. part 2: Model verification and performance," *Electrical Power Applications, IEE Proceedings*, vol. 144, pp. 123–129, 1997.

[30] J. Poza, E. Oyarbide, I. Sarasola, and M. Rodriguez, "Vector control design and experimental evaluation for the brushless doubly fed machine," *Electrical Power Applications, IET Proceedings*, vol. 3, no. 4, pp. 247–256, 2009.

[31] M. Yousefian, H. A. Zarchi, and H. Gorginpour, "Modified steady-state modelling of brushless doubly-fed induction generator taking core loss components into account," *IET Electric Power Applications*, vol. 13, no. 9, pp. 1402–1412, 2019.

[32] J. Du, L. Han, H. Li, X. Ou, and X. Han, "Experimental study of steady state performances about brushless doubly-fed machine of cage rotor with public bar and public end ring," in *22nd International Conference on Electrical Machines and Systems (ICEMS)*, 2019, pp. 1–6.

[33] T. Logan, J. Warrington, S. Shao, and R. McMahon, "Practical deployment of the brushless doubly-fed machine in a medium scale wind turbine," in *International Conference on Power Electronics and Drive Systems (PEDS)*, 2009, pp. 470–475.

[34] H. Gorginpour, B. Jandaghi, H. Oraee, and E. Abdi, "Magnetic equivalent circuit modelling of brushless doubly-fed induction generator," *IET Renewable Power Generation*, vol. 8, no. 3, pp. 334–346, 2014.

[35] P. J. Tavner, M. Jagiela, T. Chick, and E. Abdi-Jalebi, "A brushless doubly-fed machine for use in an integrated motor/converter, considering the rotor flux," in *3rd IEE International Conference on Power Electronics, Machines and Drives (PEMD2006)*, Dublin, April 2006.

[36] S. Abdi, E. Abdi, and R. McMahon, "A light-weight rotor design for brushless doubly fed machines," in *XIII International Conference on Electrical Machines (ICEM)*, 2018, pp. 493–498.

[37] S. Abdi, D. Llano, E. Abdi, P. Malliband, and R. McMahon, "Experimental analysis of noise and vibration for large brushless doubly fed machines," *The Journal of Engineering*, vol. 2017, no. 13, pp. 724–728, 2017.

[38] A. Oraee, E. Abdi, S. Abdi, R. McMahon, and P. J. Tavner, "Effects of rotor winding structure on the bdfm equivalent circuit parameters," *IEEE Transactions on Energy Conversion*, vol. 30, no. 4, pp. 1660–1669, 2015.

[39] S. Abdi, A. Oraee, E. Abdi, and R. McMahon, "A new optimized rotor design for brushless doubly fed machines," in *20th International Conference on Electrical Machines and Systems (ICEMS)*, 2017, pp. 1–6.

[40] F. Zhang, S. Yu, Y. Wang, S. Jin, and M. G. Jovanovic, "Design and performance comparisons of brushless doubly fed generators with different rotor structures," *IEEE Transactions on Industrial Electronics*, vol. 66, no. 1, pp. 631–640, 2019.

[41] F. Xiong and X. Wang, "Design of a low-harmonic-content wound rotor for the brushless doubly fed generator," *IEEE Transactions on Energy Conversion*, vol. 29, no. 1, pp. 158–168, 2014.

[42] P. Tavner, R. McMahon, P. Roberts, E. Abdi-Jalebi, X. Wang, M. Jagiela, and T. Chick, "Rotor design & performance for a bdfm," in *XVII international conference on electrical machines*, 2006.

[43] C. D. Cook and B. H. Smith, "Stability and stabilisation of doubly-fed single frame cascade induction machines," *IEE Proceedings*, vol. 126, no. 11, pp. 1168–1174, 1979.

[44] P. C. Roberts, R. A. McMahon, P. J. Tavner, J. M. Maciejowski, and T. J. Flack, "Equivalent circuit for the brushless doubly fed machine (bdfm) including parameter estimation and experimental verification," *Electrical Power Applications, IEE Proceedings*, vol. 152, no. 4, pp. 933–942, July 2005.

[45] S. Abdi and E. Abdi, "Simplified experimental estimation of equivalent circuit parameters for brushless doubly fed machines," in *49th Annual Conference of the IEEE Industrial Electronics Society, IECON 2023*, Singapore, 2023, pp. 1–5.

[46] R. A. McMahon, M. E. Mathekga, X. Wang, and M. R. Tatlow, "Design considerations for the brushless doubly-fed (induction) machine," *IET Electric Power Applications*, vol. 10, no. 5, pp. 394–402, 2016.

[47] E. Abdi, A. Oraee, S. Abdi, and R. A. McMahon, "Design of the brushless dfig for optimal inverter rating," in *7th IET International Conference on Power Electronics, Machines and Drives (PEMD 2014)*, 2014, pp. 1–6.

[48] A. Oraee, E. Abdi, S. Abdi, and R. McMahon, "A study of converter rating for brushless dfig wind turbines," in *2nd IET Renewable Power Generation Conference (RPG 2013)*, 2013, pp. 1–4.

[49] S. Shao, E. Abdi, and R. McMahon, "Low-cost variable speed drive based on a brushless doubly-fed motor and a fractional unidirectional converter," *IEEE Transactions on Industrial Electronics*, vol. 59, no. 1, pp. 317–325, 2012.

[50] R. McMahon, P. Roberts, M. Tatlow, E. Abdi, A. Broekhof, and S. Abdi, "Rotor parameter determination for the brushless doubly fed (induction) machine," *IET Electric Power Applications*, vol. 9, no. 8, pp. 549–555, 2015.

[51] M. Hashemnia, F. Tahami, and E. Oyarbide, "Investigation of core loss effect on steady-state characteristics of inverter fed brushless doubly fed

machines," *IEEE Transactions on Energy Conversion*, vol. 29, no. 1, pp. 57–64, March 2014.

[52] S. Abdi, E. Abdi, and H. Toshani, "Rotational iron losses in brushless doubly fed machines," in *International Conference on Electrical Machines (ICEM)*, Spain, 2022, pp. 1682–1688.

[53] S. Abdi, E. Abdi, A. Oraee, and R. McMahon, "Equivalent circuit parameters for large brushless doubly fed machines (bdfms)," *IEEE Transactions on Energy Conversion*, vol. 29, no. 3, pp. 706–715, 2014.

[54] S. Abdi, E. Abdi, and R. McMahon, "Numerical analysis of stator magnetic wedge effects on equivalent circuit parameters of brushless doubly fed machines," in *XIII International Conference on Electrical Machines (ICEM)*, 2018, pp. 879–884.

[55] R. A. McMahon, P. C. Roberts, X. Wang, and P. J. Tavner, "Performance of bdfm as generator and motor," *Electrical Power Applications, IEE Proceedings*, vol. 153, no. 2, pp. 289–299, March 2006.

[56] S. Tohidi, P. Tavner, R. McMahon, H. Oraee, M. Zolghadri, S. Shao, and E. Abdi, "Low voltage ride-through of dfig and brushless dfig: Similarities and differences," *Electric Power Systems Research*, vol. 110, pp. 64–72, 2014.

[57] E. Abdi-Jalebi and R. McMahon, "Application of real-time rotor current measurements using bluetooth wireless technology in study of the brushless doubly-fed (induction) machine (bdfm)," in *41st IEEE Industry Applications Society Annual Meeting*, vol. 3, 2006, pp. 1557–1561.

[58] D. X. Llano, S. Abdi, M. Tatlow, E. Abdi, and R. A. McMahon, "Energy harvesting and wireless data transmission system for rotor instrumentation in electrical machines," *IET Power Electronics*, vol. 10, no. 11, pp. 1259–1267, 2017.

[59] P. C. Roberts, T. Long, R. A. McMahon, S. Shao, E. Abdi, and J. M. Maciejowski, "Dynamic modelling of the brushless doubly fed machine," *IET Electric Power Applications*, vol. 7, no. 7, pp. 544–556, 2013.

[60] P. C. Roberts, "A study of brushless doubly-fed (induction) machines," Ph.D. dissertation, University of Cambridge, 2005. [Online]. Available: https://www.repository.cam.ac.uk/handle/1810/251955

[61] E. Abdi, "Modelling and instrumentation of brushless doubly-fed (induction) machines," Ph.D. dissertation, University of Cambridge, 2006. [Online]. Available: http://dx.doi.org/10.13140/RG.2.2.22175.48809

[62] M. Jevons, *Electrical Machine Theory*. London: Blackie & Son Limited, 1966.

[63] E. Abdi-Jalebi and R. McMahon, "High-performance low-cost rogowski transducers and accompanying circuitry," *IEEE Transactions on Instrumentation and Measurement*, vol. 56, no. 3, pp. 753–759, 2007.

[64] E. Abdi-Jalebi and R. A. McMahon, "Simple and practical construction of high-performance, low-cost rogowski transducers and accompanying circuitry for research applications," in *IEEE Instrumentationand Measurement Technology Conference Proceedings*, vol. 1, 2005, pp. 354–358.

[65] E. Abdi-Jalebi, P. Roberts, and R. McMahon, "Real-time rotor bar current measurement using a rogowski coil transmitted using wireless technology," in *18th International Power Systems Conference*, Tehran, Iran, October 2003.

[66] T. D. Garnett, R. A. McMahon, and E. Abdi-Jalebi, "Applications of zig-bee wireless technology for industrial instrumentation," in *Proceedings of the 41st International Universities Power Engineering Conference*, vol. 2, 2006, pp. 748–752.

[67] S. Shao, E. Abdi, F. Barati, and R. McMahon, "Stator-flux-oriented vector control for brushless doubly fed induction generator," *IEEE Transactions on Industrial Electronics*, vol. 56, no. 10, pp. 4220–4228, 2009.

Ehsan Abdi is the founder and director of Wind Technologies Limited in Cambridge, where he has led the commercialisation of the brushless doubly-fed machine for wind power applications. He graduated from Cambridge University with the MPhil and PhD degrees in Electrical Engineering in 2003 and 2006, respectively. He obtained his BSc degree in the same subject from Sharif University of Technology in Iran in 2002. Dr Abdi has received several prestigious awards and recognitions, among which are The Scientific Instrument Maker Award, runner-up for the IET Innovation in Engineering Award, and IET Young Professional Paper Award. His main research interests include electrical machines and drives, electric vehicles, wind power generation, and electrical measurements and instrumentation.

Salman Abdi received the BSc degree from Ferdowsi University, Mashhad, Iran in 2009, the MSc degree from Sharif University of Technology, Tehran, Iran in 2011, both in electrical engineering, and the PhD degree in electrical machines design and optimisation from Cambridge University, UK in 2015. He is currently an Assistant Professor in electrical engineering with the University of East Anglia, Norwich, UK. His research interests revolve around electrical machine design, modelling, and instrumentation for renewable power generation and electric propulsion systems.

Richard McMahon received the degrees of BA (in Electrical Sciences) and PhD from Cambridge University in 1976 and 1980 respectively. Following postdoctoral work on semiconductor device processing, he became a University Lecturer in electrical engineering in 1989 with the Engineering Department, University of Cambridge, where he was a Senior Lecturer in 2000. Since 2016, he is with the Warwick Manufacturing Group, University of Warwick, Coventry, UK, as a Professor of Electrical Power Conversion. His current research interests include electric machines and power electronics.

Peter Tavner received the M.A. degree in engineering sciences from Cambridge University, UK in 1969, and the PhD degree in electrical engineering from Southampton University, Southampton, UK in 1978. He is currently a Professor of New and Renewable Energy with the School of Engineering, University of Durham, Durham, UK. He has held a number of research and technical positions in industry, including Technical Director of Laurence Scott Electromotors Ltd., Norwich, UK., Electromotors Ltd., and Brush Electrical Machines Ltd., Loughborough, UK. Most recently, he has been the Group Technical Director of FKI Energy Technology, Loughborough, UK. His current research interests include electrical machines for the extraction of energy from renewable sources and their connection to electricity systems and electromagnetic analysis, the application of condition monitoring to electrical systems, and the use of converters with electrical machines. Prof Tavner is a winner of the Institution Premium of the Institution of Electrical Engineers, UK.